Interference Alignment in a Poisson Field of MIMO Femtocells

Tri Minh Nguyen, Youngmin Jeong, *Student Member, IEEE*, Tony Q. S. Quek, *Senior Member, IEEE*, Wee Peng Tay, *Member, IEEE*, and Hyundong Shin, *Senior Member, IEEE*

***Abstract*—The need for bandwidth and the incitation to reduce power consumption lead to the reduction of cell size in wireless networks. This allows reducing the distance between a user and the base station, thus increasing the capacity. A relatively inexpensive way of deploying small-cell networks is to use femtocells. However, the reduction in cell size causes problems for coordination and network deployment, especially due to the intra- and cross-tier interference. In this paper, we consider a two-tier multiple-input multiple-output (MIMO) network in the downlink, where a single macrocell base station with multiple transmit antennas coexists with multiple closed-access MIMO femtocells. With multiple receive antennas at both the macrocell and femtocell users, we propose an opportunistic interference alignment scheme to design the transmit and receive beamformers in order to mitigate intra- (or inter-) and cross-tier interference. Moreover, to reduce the number of macrocell and femtocell users coexisting in the same spectrum, we apply a random spectrum allocation on top of the opportunistic interference alignment. Using stochastic geometry, we analyze the proposed scheme in terms of the distribution of a received signal-to-interference-plus-noise ratio, spatial average capacity, network throughput, and energy efficiency. In the presence of imperfect channel state information, we further quantify the performance loss in spatial average capacity. Numerical results show the effectiveness of our proposed scheme in improving the performance of random MIMO femtocell networks.**

***Index Terms*—Beamforming, femtocell network, interference alignment, interference channel, multiple-input multiple-output, random spectrum allocation, stochastic geometry.**

I. Introduction

ENERGY consumption and electromagnetic pollution are becoming societal and economic challenges of prime importance that both developed and developing countries have to tackle. The evolution of future communication infrastructures will have to take into consideration both the aforementioned factors [1]. On the other hand, the increasing demand for bandwidth-hungry multimedia and wireless services has spurred the need towards maximal exploitation of spectral resources in all available dimensions. With the need to reduce power consumption and to reuse spectral resources efficiently, there is an increasing trend towards the deployment of femtocell networks by overlaying a traditional single-cell, single-tier network with multi-tier networks with very high throughput per network area [2].

A femtocell is a low-power home base station intended for short range communications. It extends the cellular network coverage, and provides high speed data services to indoor users [3], [4]. Such small-cell networks are attractive to wireless operators since femtocells are deployed at the user premises and they leverage on the user's existing broadband internet connection as backhaul. In this way, there is no additional deployment cost, energy supply cost or site rental incurred by the operator. Although this cell-size reduction offers theoretically higher capacity and energy efficiency, it increases the complexity of all operator tasks: cell planning, site acquisition, parameters configuration and tuning, for example. As the cell density increases, classical offline planning techniques based on frequency/space reuse, power control, and antenna tilting are not able to cope with interference due to the increasing number of devices. Therefore, interference management is critical for successful deployment of femtocells and a guaranteed quality-of-service (QoS) for macrocell traffic [5]–[8].

In closed-access systems, only a subset of users defined by the femtocell owner can connect to the femtocell. Compared to open-access systems, the closed-access system is more secured and has lower network overhead. However, one drawback of the closed-access system is the vulnerability to cross-tier interference [9], [10]. Recently, the concept of interference alignment (IA) was introduced as a linear beamforming technique to align beamforming matrices at the transmitters such that the interference at each receiver is aligned in an interference subspace, leaving the desired signal to transmit in an interference-free subspace [11], [12]. At the receivers, we can apply a simple zero-forcing (ZF) receiving vector to project the desired signal onto the interference-free subspace, which is sufficient for signal detection. For instance, there is great interest in employing this concept of IA in different types of interference networks [13]–[17]. In particular, [15] proposed a combination of IA and interference cancellation to mitigate cross-tier interference. In [16], a combination of

Manuscript received January 4, 2012; revised June 10, 2012 and October 26, 2012; accepted December 20, 2012. The associate editor coordinating the review of this paper and approving it for publication was X. Gao. This paper was presented in part at the European Wireless Conference, Poznan, Poland, April 2012 and the IEEE International Symposium on Information Theory, Cambridge, MA, July 2012. This research was supported, in part, by the National Research Foundation of Korea (NRF) grant funded by the Korea government (MEST) (No. 2012-0005091 and No. 2012-0000919), SRG ISTD 2012037, CAS Fellowship for Young International Scientists Grant 2011Y2GA02, and SUTD-MIT International Design Centre under Grant IDSF1200106OH.

T. M. Nguyen, Y. Jeong, and H. Shin (Corresponding Author) are with the Department of Electronics and Radio Engineering, Kyung Hee University, 1732 Deogyeong-daero, Giheung-gu, Yongin-si, Gyeonggi-do 446-701, Korea (e-mail: {tringuyen, yjeong, hshin}@khu.ac.kr).

T. Q. S. Quek is with the Singapore University of Technology and Design, and the Institute for Infocomm Research, Singapore (e-mail: tonyquek@sutd.edu.sg).

W. P. Tay is with the Nanyang Technological University, Singapore (e-mail: wptay@ntu.edu.sg).

Digital Object Identifier xxx.

IA and the scheduling algorithm was proposed to mitigate cross-tier interference. In [17], downlink IA was employed for cognitive femtocell access points (FAPs) to improve femtocell throughput. In all these related work, the random locations of FAPs are not considered and the effect of imperfect channel state information (CSI) for IA was not accounted for.

In this paper, we consider a two-tier multiple-input multiple-output (MIMO) network in the downlink, where a single macrocell base station (MBS) with multiple transmit antennas coexists with several closed-access MIMO FAPs. With multiple receive antennas at both the macrocell and femtocell users, we propose an opportunistic IA scheme to design the transmit and receive beamformers in order to mitigate intra-, inter-, and/or cross-tier interference. Moreover, to reduce the number of macrocell and femtocell users coexisting in the same spectrum, we apply a random spectrum allocation on top of the opportunistic IA scheme. Closely related to our work is [15], where IA was combined with interference cancellation to mitigate the cross-tier interference in heterogeneous networks. In contrast, our proposed scheme takes into account the random spatial model of FAPs as well as the dense deployment of femtocell networks. Using stochastic geometry, we evaluate the performance of the proposed scheme in terms of the distribution of a received signal-to-interference-plus-noise ratio (SINR), spatial average capacity, network throughput, and energy efficiency. In the presence of imperfect CSI, we further quantify the performance loss in spatial average capacity. Numerical results show the effectiveness of our proposed scheme in improving the performance of random MIMO femtocell networks.

The paper is organized as follows. In Section II, we present our system model. In Section III, we describe our proposed interference alignment scheme. In Section IV, the performance analysis of the proposed interference coordination scheme is provided. In Section V, we investigate the effect of imperfect CSI on the proposed IA scheme. Some numerical results are provided in Section VI. Finally, the conclusion is given in Section VII. Throughout the paper, we shall use the following notation. Boldface upper-case letters denote matrices, boldface lower-case letters denote column vectors, and plain lower-case letters denote scalars. The superscripts $(\cdot)^T$, $(\cdot)^*$, and $(\cdot)^\dagger$ denote the transpose, complex conjugate, and transpose conjugate, respectively. We denote $\mathbf{I}_n$ as the $n \times n$ identity matrix, $\mathrm{tr}(\cdot)$ as the trace operator, and $\|\cdot\|$ as the standard Euclidean norm. We denote the nonnegative and positive orthants in the Euclidean vector space of dimension K by $\mathbb{R}_+^K$ and $\mathbb{R}_{++}^K$, respectively.

II. System Model

We consider a two-tier network with a central M_1-antenna MBS serving a circular region $\mathcal{C}$ of radius r_1. The macrocell is underlaid with a random number of M_2-antenna FAPs. The FAPs are spatially distributed according to a homogeneous Poisson point process (PPP) Π_0 with intensity λ. Therefore, the average number of FAPs within the cellular coverage is given by $L = \lambda |\mathcal{C}|$. For each FAP, we consider a circular cell coverage of radius r_2, where n_2 femtocell users (FUEs) are uniformly distributed on the circumference of each cell such that $r_2 \ll r_1$.[1]

A. Macrocell Tier

Assume that the available spectrum is split into B subchannels, each with bandwidth W hertz (Hz) and the MBS uses all these subchannels to serve n_1 macrocell users (MUEs) equipped with N antennas in the macrocell tier. Furthermore, we divide n_1 MUEs into macrocell user groups, such that each user group consists of ℓ MUEs sharing b subchannels. Let $\mathcal{G}$ be a group of MUEs that contains ℓ MUEs. To avoid interference among each macrocell user group, we then consider that the b subchannels allocated to each group are mutually orthogonal. Therefore, by employing multiuser MIMO, the MBS can serve all the ℓ MUEs simultaneously within each MUE group for a given set of b subchannels.

B. Femtocell Tier

In the femtocell tier, the FAPs use the frequency-ALOHA (F-ALOHA) spectrum access strategy, where each FAP has access exactly to one group of b subchannels among B ones with independent and equal probability. Therefore, the F-ALOHA thins the average number of FAPs in each subchannel by the spectrum access probability $p = b/B$. Within each FAP, we employ time-division multiple-access (TDMA) as the multiple-access scheme to serve one N-antenna FUE at each time slot for a chosen set of b subchannels. Hence, the average number of active users within the cellular coverage becomes $n_1 + pL$. In other words, for a given time slot and a given group of b subchannels, there will be ℓ MUEs coexisting with a random number of FUEs that are spatially distributed according to the PPP Π with the thinned intensity $p\lambda$.

C. Channel Model

In both tiers, the downlink channel is characterized by a path loss and Rayleigh fading. The path loss function at a distance r is equal to $r^{-\alpha}$, where α is the path loss exponent. In what follows, we denote α_1, α_2, and α_3 as the path loss exponents of the outdoor link, the indoor link, and the cross link between indoor and outdoor, respectively. For the macrocell tier, we denote $\mathbf{G}_{1i} \in \mathbb{C}^{N \times M_1}$ and $\mathbf{G}_{2i} \in \mathbb{C}^{N \times M_1}$ as the random channel matrices from the MBS to the ith MUE and to the FUE of the ith FAP, respectively. For the femtocell tier, we denote $\mathbf{H}_{ij} \in \mathbb{C}^{N \times M_2}$ and $\mathbf{K}_{ij} \in \mathbb{C}^{N \times M_2}$ as the random channel matrices from the jth FAP to the ith FUE and MUE, respectively.[2] Note that each entry of the channel matrices $\mathbf{G}_{1i}$, $\mathbf{G}_{2i}$, $\mathbf{H}_{ij}$, and $\mathbf{K}_{ij}$ is distributed as $\mathcal{CN}(0, 1)$.[3]

[1] As the radius r_1 of macrocell tier is sufficiently large, we can ignore the edge effects in our analysis.

[2] In what follows, we simply denote 'the FUE of the ith FAP' by 'the ith FUE'.

[3] $\mathcal{CN}(\mu, \sigma^2)$ denotes a circularly symmetric complex Gaussian distribution with mean μ and variance σ^2.

D. Signal Model

We consider a typical receiver in each tier, denoted by the MUE 0 and FUE 0, respectively. The MBS and each FAP transmit the single stream signal to its serving users with a beamforming strategy. Let $\mathbf{f}_i \in \mathbb{C}^{M_1}$ be the transmit beamforming vector from the MBS to the ith MUE and $\mathbf{v}_i \in \mathbb{C}^{M_2}$ be the transmit beamforming vector from the ith FAP to its own FUE. Then, the received signal at the typical MUE 0 within the group $\mathcal{G}$ can be written as

$$\mathbf{y}_{10} = \underbrace{D_1^{-\alpha_1/2}\mathbf{G}_{10}\mathbf{f}_0 x_0}_{\text{(desired signal)}} + \underbrace{\sum_{i\in\Pi} R_{1i}^{-\alpha_3/2}\mathbf{K}_{0i}\mathbf{v}_i s_i}_{\text{(cross-tier interference)}} + \underbrace{\sum_{j\in\mathcal{G}\setminus\{0\}} D_1^{-\alpha_1/2}\mathbf{G}_{10}\mathbf{f}_j x_j}_{\text{(inter-tier interference)}} + \mathbf{n}_1 \tag{1}$$

and similarly at the typical FUE 0 as

$$\mathbf{y}_{20} = \underbrace{r_2^{-\alpha_2/2}\mathbf{H}_{00}\mathbf{v}_0 s_0}_{\text{(desired signal)}} + \underbrace{\sum_{i\in\Pi\setminus\{0\}} R_{2i}^{-\alpha_3/2}\mathbf{H}_{0i}\mathbf{v}_i s_i}_{\text{(intra-tier interference)}} + \underbrace{\sum_{j\in\mathcal{G}} D_2^{-\alpha_1/2}\mathbf{G}_{20}\mathbf{f}_j x_j}_{\text{(cross-tier interference)}} + \mathbf{n}_2 \tag{2}$$

where D_1 and D_2 are the distances from the MBS to the typical MUE and FUE receivers, respectively; R_{1i} and R_{2i} are the distances from the ith FAP to the typical MUE and FUE, respectively; $x_i \in \mathbb{C}$ and $s_i \in \mathbb{C}$ are the desired signals for the ith MUE and FUE within the group $\mathcal{G}$ such that $\mathbb{E}\left\{|x_i|^2\right\} = P_1$ and $\mathbb{E}\left\{|s_i|^2\right\} = P_2$, respectively; and $\mathbf{n}_1$ and $\mathbf{n}_2$ are the N-dimensional complex additive white Gaussian noise (AWGN) vectors with zero mean and covariance $N_0\mathbf{I}_N$. Let the (receive) beamforming vectors at the ith MUE and FUE be $\mathbf{u}_i \in \mathbb{C}^N$ and $\mathbf{w}_i \in \mathbb{C}^N$, respectively. Then, after receive beamforming, we get

$$\mathbf{u}_0^{\dagger}\mathbf{y}_{10} \tag{3}$$

$$\mathbf{w}_0^{\dagger}\mathbf{y}_{20} \tag{4}$$

at the typical MUE and FUE, respectively.

III. Opportunistic Interference Alignment

Using IA, we align the interference from the intra- and cross-tier networks into some received signal subspace so that we can beamform to nullify the interference and detect the desired signal in other interference-free subspace. However, due to the large number of FAPs and their random deployment, it is challenging to suppress all the interference from the FAPs. Instead, we develop opportunistic IA that only cancels the nearest interferer.

Algorithm 1 (Opportunistic IA): The description of opportunistic IA is given as follows:

Step 1 For a given set of subchannels, the ith MUE in the set $\mathcal{G}$ of ℓ MUEs first identifies the set $\mathcal{N}_i$ of the nearest interfering FAPs to design its ZF receiving vector $\mathbf{u}_i$ such that it is orthogonal to all these interfering links. This is feasible only if

$$|\mathcal{N}_i| + 1 \le N. \tag{5}$$

When (5) holds, the receive beamforming vector at MUE i is given by

$$\mathbf{u}_i \in \mathsf{Null}\left(\bigcup_{i\in\mathcal{G},\, j\in\mathcal{N}_i} \mathbf{K}_{ij}\mathbf{v}_j\right). \tag{6}$$

Step 2 Next, we design the transmit beamforming vectors at the MBS such that the ℓ MUEs are mutually orthogonal to each other. Since the receive beamforming vectors of the ℓ MUEs have already been determined in Step 1, we should take them into account in the design of transmit beamforming vectors as follows:

$$\mathbf{f}_i \in \mathsf{Null}\left(\bigcup_{j\in\mathcal{G},\, j\neq i} \mathbf{u}_j^{\dagger}\mathbf{G}_{1j}\right). \tag{7}$$

Step 3 Now, we proceed to the design of the transmit beamforming vector at each FAP using the IA concept. Specifically, we ensure that the transmit beamforming vector is chosen such that the intra-tier interference from each FAP to its nearest victim FUE is aligned with the cross-tier interference from the MBS to this victim FUE. Therefore, the transmit beamforming vector $\mathbf{v}_j$ at FAP j should satisfy the condition

$$\mathsf{Span}\left(\mathbf{H}_{ij}\mathbf{v}_j\right) = \mathsf{Span}\left(\mathbf{G}_{2i}\sum_{k\in\mathcal{G}}\mathbf{f}_k\right) \tag{8}$$

where i is the user index of the nearest victim FUE. This is feasible only if

$$N \le M_2. \tag{9}$$

Step 4 Lastly, we need to design the receive beamforming vector at each FAP. Since the intra- and cross-tier interference has been aligned in Step 3, we can simply design the receive beamforming vector at each FUE to be orthogonal to the aligned interference subspace as follows:

$$\mathbf{w}_j \in \mathsf{Null}\left(\mathbf{G}_{2j}\sum_{k\in\mathcal{G}}\mathbf{f}_k\right). \tag{10}$$

Remark 1 (Feasibility): The feasibility of Algorithm 1 is treated in Appendix A. In addition to the feasible conditions (5) and (9) for Steps 1 and 3, we require the additional condition

$$(\ell - 1)\, N \le M_1 \tag{11}$$

for this opportunistic IA algorithm to be feasible, and this is obtained by combining (6)–(8).

Remark 2: Since the design of $\mathbf{f}_i$ depends only on the knowledge of channel information—see (69) in Appendix A—we begin the opportunistic IA algorithm by designing $\mathbf{f}_i$, followed by designing $\mathbf{v}_i$ and $\mathbf{u}_i$, and finally $\mathbf{w}_i$.

IV. Performance Analysis

In this section, we evaluate the performance of opportunistic IA (Algorithm 1) in random MIMO femtocell networks in terms of the SINR distribution, spatial average capacity, network throughput, and energy efficiency.

A. SINR Distribution and Spatial Average Capacity

1) Femtocell User: Let Ω be the random set of FAPs causing the residual intra-tier (femtocell) interference after opportunistic IA. Since the FUE is free from the cross-tier (macrocell) interference due to the opportunistic IA, (4) then becomes

$$\mathbf{w}_0^\dagger \mathbf{y}_{20} = r_2^{-\alpha_2/2} \mathbf{w}_0^\dagger \mathbf{H}_{00} \mathbf{v}_0 s_0 + \sum_{i \in \Omega} R_{2i}^{-\alpha_3/2} \mathbf{w}_0^\dagger \mathbf{H}_{0i} \mathbf{v}_i s_i + \mathbf{w}_0^\dagger \mathbf{n}_2 \quad (12)$$

so that the SINR at the typical FUE is

$$\gamma_{\text{FUE}} = \frac{P_2 r_2^{-\alpha_2} \left|\mathbf{w}_0^\dagger \mathbf{H}_{00} \mathbf{v}_0\right|^2}{P_2 \underbrace{\sum_{i \in \Omega} R_{2i}^{-\alpha_3} \left|\mathbf{w}_0^\dagger \mathbf{H}_{0i} \mathbf{v}_i\right|^2}_{\triangleq I_{\text{FUE}}(\Omega)} + N_0} \quad (13)$$

where $I_{\text{FUE}}(\Omega)$ denotes the residual intra-tier interference power from the FAP set Ω. Note that since $\|\mathbf{w}_i\| = \|\mathbf{v}_j\| = 1$, we have $\mathbf{w}_i^\dagger \mathbf{H}_{ij} \mathbf{v}_j \sim \mathcal{CN}(0,1)$, $\forall i, j$. For simplicity, we assume that each FAP has a different nearest victim FUE.

Theorem 1: Let

$$i^\star = \arg\min_{i \in \Pi \setminus \{0\}} R_{2i} \quad (14)$$

and $\mathcal{A}$ be the event that the typical FUE is capable of canceling its nearest interfering FAP $i^\star$. Then, we have

$$\mathbb{P}\left\{\mathcal{A} \middle| R_{2i^\star}\right\} = p\lambda\zeta R_{2i^\star}^2 \exp\left(-p\lambda\zeta R_{2i^\star}^2\right) \quad (15)$$

where

$$\zeta = \frac{2\pi + 3\sqrt{3}}{6}. \quad (16)$$

Proof: We provide a sketch of the proof by following the designs in Algorithm 1. From Step 1, the MUE i is free from the inter-tier interference caused by the other MUEs as well as the cross-tier interference caused by the nearest FAPs in $\mathcal{N}_i$. From Steps 3 and 4, each FUE can suppress the cross-tier interference from the MBS and the intra-tier interference from the nearest FAP. Therefore, the FUE creates its receiving matrix that lies in the null space of the cross-tier interfering signals from the MBS. However, the interfering FAP that spans the same subspace with the interfering stream from the MBS to the FUE is not always the nearest neighbor to the FUE. When this FAP is the nearest neighbor, the FUE can at the same time cancel both interference from the MBS and the nearest FAP. The event $\mathcal{A}$ is equivalent to the event that there is only one FAP in the region $\bar{\mathcal{V}}(R_{2i^\star})$ as shown in Fig. 1. Hence, we have

$$\mathbb{P}\left\{\mathcal{A} \middle| R_{2i^\star}\right\} = \mathbb{P}\left\{\text{only one FAP in } \bar{\mathcal{V}}(R_{2i^\star})\right\} = p\lambda \left|\bar{\mathcal{V}}(R_{2i^\star})\right| \exp\left(-p\lambda\left|\bar{\mathcal{V}}(R_{2i^\star})\right|\right). \quad (17)$$

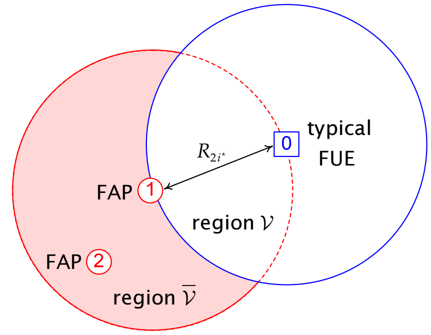

(a) Event $\mathcal{A}^c$

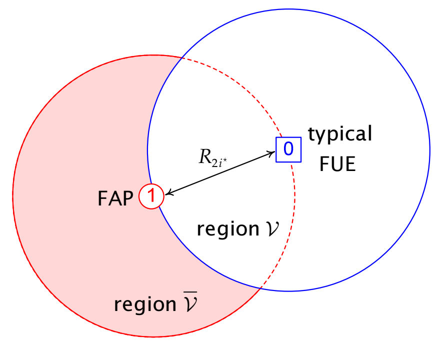

(b) Event $\mathcal{A}$

Fig. 1. Example scenarios where (a) the event $\mathcal{A}$ that the typical FUE is capable of canceling its nearest interfering FAP $i^\star$ (i.e., $i^\star = 1$) does not occur as there exist two FAPs (FAP 1 and FAP 2) in the region $\bar{\mathcal{V}}(R_{2i^\star})$; and (b) the event $\mathcal{A}$ occurs as there is only one FAP in $\bar{\mathcal{V}}(R_{2i^\star})$.

The area of the region $\bar{\mathcal{V}}(R_{2i^\star})$ is given by (see Fig. 1)

$$\left|\bar{\mathcal{V}}(R_{2i^\star})\right| = \left(\pi - \left|\mathcal{V}(R_{2i^\star})\right|\right) R_{2i^\star}^2 = \frac{2\pi + 3\sqrt{3}}{6} R_{2i^\star}^2 \quad (18)$$

which completes the proof. □

Using the alignment event $\mathcal{A}$, the cumulative distribution function (CDF) of γ_{FUE} can be written as

$$F_{\gamma_{\text{FUE}}}(z) = 1 - \mathbb{P}\left\{\gamma_{\text{FUE}} \geq z, \mathcal{A}\right\} - \mathbb{P}\left\{\gamma_{\text{FUE}} \geq z, \mathcal{A}^c\right\}, \quad z \geq 0 \quad (19)$$

where $\mathcal{A}^c$ is the complement event of $\mathcal{A}$. Then, letting $\Omega = \Pi \setminus \{0, i^\star\}$, for $z \geq 0$, we have (20), as shown at the bottom of the next page, where $\phi_{X|Y}\left(s \middle| Y\right) \triangleq \mathbb{E}\left\{e^{-sX} \middle| Y\right\}$ is the conditional moment generating function (MGF) of a random variable (RV) X given Y, which is again a RV derived from Y. Similarly, we get $\mathbb{P}\left\{\gamma_{\text{FUE}} \geq z \middle| \mathcal{A}^c\right\}$ akin to (20) by setting $\Omega = \Pi \setminus \{0\}$. Using (19), (20), and Theorem 1, we can characterize the FUE performances in terms of the SINR distribution and spatial average capacity.

Theorem 2: The opportunistic IA in Algorithm 1 achieves at the FUE the SINR distribution

$$F_{\gamma_{\rm FUE}}(z) = 1 - \int_0^\infty f(r)\, g(r, z r_2^{\alpha_2})\, dr - \left[1 - \frac{2\pi\zeta}{(\zeta+2\pi)^2}\right] g(0, z r_2^{\alpha_2}), \quad z \geq 0 \tag{21}$$

and the spatial average capacity in bits/s/Hz

$$\langle C\rangle_{\rm FUE} = \int_0^\infty \int_0^\infty f(r)\, g(r, \epsilon_t r_2^{\alpha_2})\, dr dt + \left[1 - \frac{2\pi\zeta}{(\zeta+2\pi)^2}\right] \int_0^\infty g(0, \epsilon_t r_2^{\alpha_2})\, dt \tag{22}$$

where $\epsilon_t = 2^t - 1$ and

$$f(r) = 2\pi\zeta p^2 \lambda^2 r^3 \exp\left[-(\zeta+\pi) p\lambda r^2\right] \tag{23}$$

$$g(r,s) = \exp\left[-2\pi p\lambda s \left(1 - \frac{r^2}{r_1^2}\right) \int_r^{r_1} \frac{t dt}{s + t^{\alpha_3}} - \frac{sN_0}{P_2}\right]. \tag{24}$$

Proof: See Appendix B. □

Remark 3 (Lower and Upper Bounds): The connectivity probability of the typical FUE at a rate of $\mathcal{R}$ bits/s/Hz is lower-bounded as

$$\mathbb{P}\{\log_2(1+\gamma_{\rm FUE}) > \mathcal{R}\} \geq \mathbb{P}\left\{\log_2(1+\gamma_{\rm FUE}) > \mathcal{R} \middle| \mathcal{A}^c\right\} = g(0, \epsilon_{\mathcal{R}} r_2^{\alpha_2}) \tag{25}$$

leading to

$$\langle C\rangle_{\rm FUE} \geq \int_0^\infty g(0, \epsilon_t r_2^{\alpha_2})\, dt \tag{26}$$

which is achievable from Algorithm 1 without the opportunistic IA in Step 3. Specifically, when $\alpha_3 = 4$, we have

$$g(0, \epsilon_{\mathcal{R}} r_2^{\alpha_2}) = \exp\left[-\pi p\lambda \sqrt{\epsilon_{\mathcal{R}} r_2^{\alpha_2}} \arctan\left(\frac{r_1^2}{\sqrt{\epsilon_{\mathcal{R}} r_2^{\alpha_2}}}\right) - \epsilon_{\mathcal{R}} r_2^{\alpha_2} \frac{N_0}{P_2}\right]. \tag{27}$$

On the other hand, the (FUE) connectivity probability at $\mathcal{R}$ bits/s/Hz is upper-bounded as

$$\mathbb{P}\{\log_2(1+\gamma_{\rm FUE}) > \mathcal{R}\} \leq \mathbb{P}\left\{\log_2(1+\gamma_{\rm FUE}) > \mathcal{R} \middle| \mathcal{A}\right\} = \mathbb{E}_{R_{2i^\star}}\{g(R_{2i^\star}, \epsilon_{\mathcal{R}} r_2^{\alpha_2})\} \tag{28}$$

leading to

$$\langle C\rangle_{\rm FUE} \leq \int_0^\infty \mathbb{E}_{R_{2i^\star}}\{g(R_{2i^\star}, \epsilon_t r_2^{\alpha_2})\}\, dt \tag{29}$$

which corresponds to the case that the FUE is always able to successfully cancel the cross-tier interference as well as the nearest intra-tier interference from the opportunistic IA. Again, when $\alpha_3 = 4$, we have

$$\mathbb{E}_{R_{2i^\star}}\{g(R_{2i^\star}, \epsilon_{\mathcal{R}} r_2^{\alpha_2})\} = \mathbb{E}_{R_{2i^\star}}\left\{\exp\left[-\pi p\lambda \sqrt{\epsilon_{\mathcal{R}} r_2^{\alpha_2}} \left(1 - \frac{R_{2i^\star}^2}{r_1^2}\right) \times \arctan\left(\frac{\sqrt{\epsilon_{\mathcal{R}} r_2^{\alpha_2}}\,(r_1^2 - R_{2i^\star}^2)}{\epsilon_{\mathcal{R}} r_2^{\alpha_2} + (r_1 R_{2i^\star})^2}\right) - \epsilon_{\mathcal{R}} r_2^{\alpha_2} \frac{N_0}{P_2}\right]\right\}. \tag{30}$$

2) Macrocell User: Let $\mathcal{N}_0$ be the set of the nearest interfering FAPs to the typical MUE 0 in Step 1 of Algorithm 1. Since the typical MUE is free from the inter-tier (macrocell) and the nearest cross-tier (femtocell) interference from $\mathcal{N}_0$ due to opportunistic IA, (3) then becomes

$$\mathbf{u}_0^\dagger \mathbf{y}_{10} = D_1^{-\alpha_1/2} \mathbf{u}_0^\dagger \mathbf{G}_{10} \mathbf{f}_0 x_0 + \sum_{i \in \Pi \setminus \mathcal{N}_0} R_{1i}^{-\alpha_3/2} \mathbf{u}_0^\dagger \mathbf{K}_{0i} \mathbf{v}_i s_i + \mathbf{u}_0^\dagger \mathbf{n}_1 \tag{31}$$

leading to the SINR at the typical MUE:

$$\gamma_{\rm MUE} = \frac{P_1 D_1^{-\alpha_1} \left|\mathbf{u}_0^\dagger \mathbf{G}_{10} \mathbf{f}_0\right|^2}{P_2 \sum_{i \in \Pi \setminus \mathcal{N}_0} R_{1i}^{-\alpha_3} \left|\mathbf{u}_0^\dagger \mathbf{K}_{0i} \mathbf{v}_i\right|^2 + N_0}. \tag{32}$$

Since $\|\mathbf{u}_i\| = \|\mathbf{f}_j\| = \|\mathbf{v}_j\| = 1$, we have again $\mathbf{u}_i^\dagger \mathbf{G}_{ij} \mathbf{f}_j \sim \mathcal{CN}(0,1)$ and $\mathbf{u}_i^\dagger \mathbf{K}_{ij} \mathbf{v}_j \sim \mathcal{CN}(0,1)$, $\forall i, j$.

Theorem 3: The opportunistic IA in Algorithm 1 achieves at the MUE the SINR distribution

$$F_{\gamma_{\rm MUE}}(z) = 1 - \int_0^\infty \left\{ g\left(r, \frac{z D_1^{\alpha_1} P_2}{P_1}\right) \frac{2(\pi p\lambda)^{|\mathcal{N}_0|}}{(|\mathcal{N}_0|-1)!} \times r^{2|\mathcal{N}_0|-1} e^{-\pi p\lambda r^2} \right\} dr \tag{33}$$

and the spatial average capacity in bits/s/Hz

$$\langle C\rangle_{\rm MUE} = \int_0^\infty \int_0^\infty \left\{ g\left(r, \frac{\epsilon_t D_1^{\alpha_1} P_2}{P_1}\right) \frac{2(\pi p\lambda)^{|\mathcal{N}_0|}}{(|\mathcal{N}_0|-1)!} \times r^{2|\mathcal{N}_0|-1} e^{-\pi p\lambda r^2} \right\} dr dt. \tag{34}$$

Proof: It follows readily from taking the same steps as in the proof of Theorem 2 using the PDF of the $|\mathcal{N}_0|$th nearest distance for the PPP Π with intensity $p\lambda$ [18], [19], along with the fact that the typical MUE is capable of successfully

$$\begin{aligned}\mathbb{P}\left\{\gamma_{\rm FUE} \geq z \middle| \mathcal{A}, R_{2i^\star}\right\} &= \mathbb{P}\left\{\left|\mathbf{w}_0^\dagger \mathbf{H}_{00} \mathbf{v}_0\right|^2 \geq z r_2^{\alpha_2} \left(\sum_{i \in \Omega} R_{2i}^{-\alpha_3} \left|\mathbf{w}_0^\dagger \mathbf{H}_{0i} \mathbf{v}_i\right|^2 + \frac{N_0}{P_2}\right) \middle| R_{2i^\star}\right\} \\ &= \mathbb{E}\left\{\exp\left[-z r_2^{\alpha_2} \left(I_{\rm FUE}(\Omega) + \frac{N_0}{P_2}\right)\right] \middle| R_{2i^\star}\right\} \\ &= \exp\left(-z r_2^{\alpha_2} \frac{N_0}{P_2}\right) \phi_{I_{\rm FUE}(\Omega)|R_{2i^\star}}\left(z r_2^{\alpha_2} \middle| R_{2i^\star}\right)\end{aligned} \tag{20}$$

canceling the inter-tier interference as well as the $|\mathcal{N}_0|$ nearest cross-tier interference from the opportunistic IA. □

Remark 4: Similar to (25), the connectivity probability of the typical MUE at a rate of $\mathcal{R}$ bits/s/Hz is lower-bounded as

$$\mathbb{P}\left\{\log_2\left(1+\gamma_{\rm MUE}\right) > \mathcal{R}\right\} \geq g\left(0, \frac{\epsilon_{\mathcal{R}} D_1^{\alpha_1} P_2}{P_1}\right) \tag{35}$$

leading to

$$\langle C \rangle_{\rm MUE} \geq \int_0^\infty g\left(0, \frac{\epsilon_t D_1^{\alpha_1} P_2}{P_1}\right) dt \tag{36}$$

which is achievable from Algorithm 1 without Step 1.

B. Network Throughput

We consider that all users in the network are able to track their received SINRs in each subchannel and feedback instantaneous rates to their MBS and FAPs with negligible delay. At each MBS or FAP, we assign a transmission rate adaptively based on these feedbacks. Let Δ be the power factor (or Shannon gap) to achieve the same rate between the capacity-achieving scheme and uncoded variable-rate quadrature amplitude modulation (QAM) transmission [20]. Then, for adaptive QAM with q discrete rates, the ith instantaneous rate in bits/s/Hz is given by

$$\mathcal{R}_i = \log_2\left(1 + \frac{\mathsf{sinr}_i}{\Delta}\right) \tag{37}$$

if the SINR lies in the regime $[\mathsf{sinr}_i, \mathsf{sinr}_{i+1})$ for $i = 1, 2, \ldots, q$. At the bit error probability of $P_{\rm b}$, the Shannon gap Δ is

$$\Delta = \frac{-1.5}{\ln\left(5P_{\rm b}\right)} \tag{38}$$

which is independent of the fading distribution [20]. For example, $\Delta = 0.1229$ at $P_{\rm b} = 10^{-6}$.

For adaptive QAM with variable rates $1, 2, \ldots, q$ bits/s/Hz, the femtocell throughput in bits/s/Hz at each FUE is given by

$$\begin{aligned}\mathcal{T}_{\rm FUE} &= q\,\mathbb{P}\left\{\gamma_{\rm FUE} \geq \epsilon_q \Delta\right\} \\ &\quad + \sum_{i=1}^{q-1} i\,\mathbb{P}\left\{\epsilon_i\Delta \leq \gamma_{\rm FUE} < \epsilon_{i+1}\Delta\right\} \\ &= q - \sum_{i=1}^{q} F_{\gamma_{\rm FUE}}\left(\epsilon_i \Delta\right).\end{aligned} \tag{39}$$

Since the average number of active FUEs is pL, the aggregate femtocell throughput is equal to $pL\mathcal{T}_{\rm FUE}$. Similarly, the macrocell throughput in bits/s/Hz at each MUE is given by

$$\mathcal{T}_{\rm MUE} = q - \sum_{i=1}^{q} F_{\gamma_{\rm MUE}}\left(\epsilon_i \Delta\right). \tag{40}$$

Since there exist n_1 MUEs, the aggregate macrocell throughput is equal to $n_1\mathcal{T}_{\rm MUE}$.

Theorem 4 (Optimal FAP Density): Let

$$\mathcal{T} = n_1\mathcal{T}_{\rm MUE} + pL\mathcal{T}_{\rm FUE} \tag{41}$$

be the total network throughput in bits/s/Hz. Then, the optimal value

$$\lambda^\star = \arg\max_{\lambda\geq 0} \mathcal{T} \tag{42}$$

of the FAP density λ that maximizes the network throughput $\mathcal{T}$ is the solution of $\partial\mathcal{T}/\partial\lambda = 0$.

Proof: See Appendix C. □

C. Energy Efficiency

Let β_i and Q_i, $i = 1, 2$, be the scaling factors of the transmission power due to amplifier/feeder losses and the fixed amounts of powers due to signal processing, site cooling, etc, at the base stations (MBS and FAPs), respectively [21]. Then, the powers consumed by the MBS and each FAP are given by

$$\mathcal{P}_1 = n_1\beta_1 P_1 + Q_1 \tag{43}$$

$$\mathcal{P}_2 = \beta_2 P_2 + Q_2 \tag{44}$$

respectively. The energy efficiency $\mathcal{E}$ in bits/joule/Hz can therefore be defined as

$$\mathcal{E} = \frac{\mathcal{T}}{\mathcal{P}_1 + pL\mathcal{P}_2}. \tag{45}$$

Since the network throughput $\mathcal{T}$ as a function of the FAP density $\lambda \geq 0$ is concave (see Appendix C), the energy efficiency $\mathcal{E}$ is also a concave function in $\lambda \geq 0$. Hence, the optimal value of λ that maximizes $\mathcal{E}$ is the solution of $\partial\mathcal{E}/\partial\lambda = 0$.

V. Effects of Imperfect CSI

In practical systems, we often deal with the problem of imperfect CSI, where the transmitters and/or receivers do not have perfect CSI knowledge. In this section, we consider imperfect CSI in opportunistic IA at the MBS and FAPs. As in [22], we use an analog channel estimation model where the transmitters employ power control to recover the power loss due to distance propagation, enabling to ignore the effect of path loss components in the model. The procedure of channel estimation consists of two phases for inter- (or intra-) and cross-tier channel information.

A. Phase 1: Inter/Intra-Tier CSI

In a given group $\mathcal{G}$ of b subchannels, each MUE and FUE simultaneously broadcast a training pilot in the first phase. Specifically, the ith MUE and the jth FUE in the group $\mathcal{G}$ broadcast the pilot matrices $\mathbf{Q}_{1i} \in \mathbb{C}^{N\times J_1}$ and $\mathbf{Q}_{2j} \in \mathbb{C}^{N\times J_1}$. To avoid interference to each other in the training process, all the training pilots $\mathbf{Q}_{1i}$ and $\mathbf{Q}_{2j}$ are mutually orthogonal such that

$$\begin{cases}\mathbf{Q}_{1i}\mathbf{Q}_{1j}^\dagger = \delta_{ij}\mathbf{I}_N \\ \mathbf{Q}_{2i}\mathbf{Q}_{2j}^\dagger = \delta_{ij}\mathbf{I}_N \\ \mathbf{Q}_{1i}\mathbf{Q}_{2j}^\dagger = \mathbf{0}_{N\times N}\end{cases} \tag{46}$$

for all i, j, where $J_1 = (\ell + |\Pi|)\,N$ and

$$\delta_{ij} = \begin{cases}1, & i = j \\ 0, & i \neq j.\end{cases} \tag{47}$$

TABLE I
TWO-PHASE CHANNEL ESTIMATION PROCEDURE

	MBS			FAP j		
	Power	Channel	Message	Power	Channel	Message
MUE i	η_1	$\mathbf{G}_{1i}^T$	$\mathbf{Q}_{1i}$	η_1	$\mathbf{K}_{ij}^T$	$\mathbf{Q}_{1i}$
FUE i	η_2	$\mathbf{G}_{2i}$	$\mathbf{Q}_{2i}$	η_2	$\mathbf{H}_{ij}^T$	$\mathbf{Q}_{2i}$
Phase 1	$\widehat{\mathbf{G}}_{1i}^T$ (Inter-tier CSI, $\forall i \in \mathcal{G}$)			$\widehat{\mathbf{H}}_{ij}^T$ (Intra-tier CSI, $\forall i \in \Pi$)		
MUE i	$\tilde{\eta}_1$	$\mathbf{G}_{1i}^T$	$\mathbf{X}_i\mathbf{\Lambda}_{1i}$	$\tilde{\eta}_1$	$\mathbf{K}_{ij}^T$	$\mathbf{X}_i\mathbf{\Lambda}_{1i}$
FUE i	$\tilde{\eta}_2$	$\mathbf{G}_{2i}$	$\mathbf{S}_i\mathbf{\Lambda}_{2i}$	$\tilde{\eta}_2$	$\mathbf{H}_{ij}^T$	$\mathbf{S}_i\mathbf{\Lambda}_{2i}$
Phase 2	$\widehat{\mathbf{X}}_i = \widehat{\mathbf{K}}_{ii_\star}$ (Cross-tier CSI, $\forall i \in \mathcal{G}$)			$\widehat{\mathbf{S}}_i = \widehat{\mathbf{G}}_{2i}$ (Cross-tier CSI, $\forall i \in \Pi$)		

Then, the received matrices at the MBS and FAP j for pilot transmission in Phase 1 can be written respectively as[4]

$$\mathbf{Y}_1^{(1)} = \sum_{i\in\mathcal{G}} \sqrt{\eta_1}\mathbf{G}_{1i}^T\mathbf{Q}_{1i} + \sum_{j\in\Pi} \sqrt{\eta_2}\mathbf{G}_{2j}^T\mathbf{Q}_{2j} + \mathbf{N}_1^{(1)} \tag{48}$$

$$\mathbf{Y}_{2j}^{(1)} = \sum_{i\in\Pi} \sqrt{\eta_2}\mathbf{H}_{ij}^T\mathbf{Q}_{2i} + \sum_{k\in\mathcal{G}} \sqrt{\eta_1}\mathbf{K}_{kj}^T\mathbf{Q}_{1k} + \mathbf{N}_2^{(1)} \tag{49}$$

where $\eta_1 = P_1(\ell + pL)$ and $\eta_2 = P_2(\ell + pL)$ are the pilot transmission powers at the MUE and FUE, respectively; and $\mathbf{N}_1^{(1)} \in \mathbb{C}^{M_1\times J_1}$ and $\mathbf{N}_2^{(1)} \in \mathbb{C}^{M_2\times J_1}$ are the AWGN matrices whose entries are independent complex Gaussian $\mathcal{CN}(0, N_0)$.

Using a linear minimum mean-square error (MMSE) estimator, the MBS and FAP j obtain the estimates of the inter- and intra-tier channels $\mathbf{G}_{1i}^T$ ($\forall i \in \mathcal{G}$) and $\mathbf{H}_{ij}^T$ ($\forall i \in \Pi$), respectively, as follows:

$$\widehat{\mathbf{G}}_{1i}^T = \frac{\sqrt{\eta_1}}{\eta_1 + N_0}\mathbf{Y}_1^{(1)}\mathbf{Q}_{1i}^\dagger \tag{50}$$

$$\widehat{\mathbf{H}}_{ij}^T = \frac{\sqrt{\eta_2}}{\eta_2 + N_0}\mathbf{Y}_{2j}^{(1)}\mathbf{Q}_{2i}^\dagger. \tag{51}$$

It follows from (46)–(51) that the entries of the channel estimate $\widehat{\mathbf{G}}_{1i}^T$ are independent Gaussian $\mathcal{CN}\big(0, \frac{1}{1+N_0/\eta_1}\big)$, whereas the entries of $\widehat{\mathbf{H}}_{ij}^T$ are independent $\mathcal{CN}\big(0, \frac{1}{1+N_0/\eta_2}\big)$. Similarly, letting

$$\widetilde{\mathbf{G}}_{1i}^T = \mathbf{G}_{1i}^T - \widehat{\mathbf{G}}_{1i}^T \tag{52}$$

$$\widetilde{\mathbf{H}}_{ij}^T = \mathbf{H}_{ij}^T - \widehat{\mathbf{H}}_{ij}^T \tag{53}$$

be the estimation errors, we have that the entries of $\widetilde{\mathbf{G}}_{1i}^T$ and $\widetilde{\mathbf{H}}_{ij}^T$ are independent Gaussian $\mathcal{CN}\big(0, \frac{1}{1+\eta_1/N_0}\big)$ and $\mathcal{CN}\big(0, \frac{1}{1+\eta_2/N_0}\big)$, respectively. Note that the estimation errors vanish as η_1/N_0 and η_2/N_0 tend to infinity—leading to perfect CSI.

B. Phase 2: Cross-Tier CSI

For simplicity, we consider that the MUE $i \in \mathcal{G}$ attempts to suppress cross-tier interference from only its nearest interfering FAP $i_\star$ in the algorithm design, i.e., $|\mathcal{N}_i| = 1$ in Algorithm 1. After estimating the inter- or intra-tier channels, each MUE and FUE simultaneously broadcast analog cross-tier channel information in the second phase. Specifically, the ith MUE and the jth FUE broadcast channel information

$$\mathbf{X}_i = \mathbf{K}_{ii_\star} \tag{54}$$

$$\mathbf{S}_j = \mathbf{G}_{2j} \tag{55}$$

respectively. Again, for all MUEs and FUEs to transmit simultaneously without causing mutual interference, the ith MUE and the jth FUE use unitary precoding matrices $\mathbf{\Lambda}_{1i} \in \mathbb{C}^{M_1\times J_2}$ and $\mathbf{\Lambda}_{2j} \in \mathbb{C}^{M_2\times J_2}$, respectively, satisfying

$$\begin{cases} \mathbf{\Lambda}_{1i}\mathbf{\Lambda}_{1j}^\dagger = \delta_{ij}\mathbf{I}_{M_1} \\ \mathbf{\Lambda}_{2i}\mathbf{\Lambda}_{2j}^\dagger = \delta_{ij}\mathbf{I}_{M_2} \\ \mathbf{\Lambda}_{1i}\mathbf{\Lambda}_{2j}^\dagger = \mathbf{0}_{M_1\times M_2} \end{cases} \tag{56}$$

for all i, j, where $J_2 = \ell M_1 + |\Pi|\, M_2$. The received signals at the MBS and FAP j in Phase 2 can be written respectively as

$$\mathbf{Y}_1^{(2)} = \sum_{i\in\mathcal{G}} \sqrt{\tilde{\eta}_1}\mathbf{G}_{1i}^T\mathbf{X}_i\mathbf{\Lambda}_{1i} + \sum_{j\in\Pi} \sqrt{\tilde{\eta}_2}\mathbf{G}_{2j}^T\mathbf{S}_j\mathbf{\Lambda}_{2j} + \mathbf{N}_1^{(2)} \tag{57}$$

$$\mathbf{Y}_{2j}^{(2)} = \sum_{i\in\Pi} \sqrt{\tilde{\eta}_2}\mathbf{H}_{ij}^T\mathbf{S}_i\mathbf{\Lambda}_{2i} + \sum_{k\in\mathcal{G}} \sqrt{\tilde{\eta}_1}\mathbf{K}_{kj}^T\mathbf{X}_k\mathbf{\Lambda}_{1k} + \mathbf{N}_2^{(2)} \tag{58}$$

where $\tilde{\eta}_1 = P_1(\ell + pLM_2/M_1)$ and $\tilde{\eta}_2 = P_2(\ell M_1/M_2 + pL)$. The MMSE estimates of cross-tier channel information $\mathbf{X}_i$ ($\forall i \in \mathcal{G}$) at the MBS and $\mathbf{S}_i$ ($\forall i \in \Pi$) at the jth FAP are given by

$$\widehat{\mathbf{X}}_i = \widehat{\mathbf{K}}_{ii_\star} = \frac{1}{\sqrt{\tilde{\eta}_1}}\Big(\widehat{\mathbf{G}}_{1i}^*\widehat{\mathbf{G}}_{1i}^T\Big)^{-1}\widehat{\mathbf{G}}_{1i}^*\mathbf{Y}_1^{(2)}\mathbf{\Lambda}_{1i}^\dagger \tag{59}$$

$$\widehat{\mathbf{S}}_i = \widehat{\mathbf{G}}_{2i} = \frac{1}{\sqrt{\tilde{\eta}_2}}\Big(\widehat{\mathbf{H}}_{ij}^*\widehat{\mathbf{H}}_{ij}^T\Big)^{-1}\widehat{\mathbf{H}}_{ij}^*\mathbf{Y}_{2j}^{(2)}\mathbf{\Lambda}_{2i}^\dagger \tag{60}$$

respectively. In Table I, we summarize the two-phase CSI estimation procedure.

C. Example: FUE Connectivity and Capacity

Theorem 5: The opportunistic IA in Algorithm 1 with the two-phase channel estimation in Table I achieves at a rate of $\mathcal{R}$ bits/s/Hz the FUE connectivity probability (61), as shown at

[4] All the communication links are assumed to have channel reciprocity. For example, $\mathbf{G}_{1i}^T \in \mathbb{C}^{M_1\times N}$ is equal to the channel matrix from the ith MUE to the MBS.

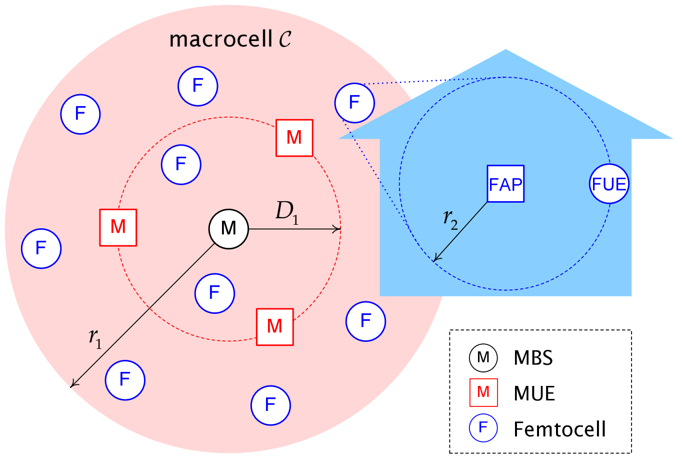

Fig. 2. A network topology for numerical examples.

TABLE II
SYSTEM PARAMETERS

Parameter	Symbol	Value
Macrocell radius	r_1	1 Km
Femtocell radius	r_2	30 m
MBS-to-MUE distance	D_1	500 m
Number of MUEs in $\mathcal{C}$	n_1	150
Number of MUEs in $\mathcal{G}$	ℓ	3
MBS antennas	M_1	4
FAP antennas	M_2	2
MUE/FUE antennas	N	2
MBS transmission power	P_1	43 dBm
FAP transmission power	P_2	23 dBm
Outdoor path loss exponent	α_1	3.8
Indoor path loss exponent	α_2	3.0
Indoor-to-outdoor path loss exponent	α_3	3.8
Shannon gap	Δ	0.1229
Noise power spectral density	N_0	10^{-8}

the bottom of the page, leading to the spatial average capacity in bits/s/Hz (62), as shown at the bottom of the page, where

$$\sigma^2 = \frac{N_0}{(M_1+M_2-N)\,P_2} \times \left[\frac{M_2}{\ell+pL} + \frac{(M_1+M_2)N}{\ell M_1 + pLM_2}\left(1+\frac{N_0}{(\ell+pL)\,P_2}\right)\right]. \quad (63)$$

Proof: See Appendix D. □

Remark 5 (Imperfectness): In (61) and (62), the factor in exponents

$$\frac{1}{1+\eta_2/N_0} + \ell\sigma^2 \quad (64)$$

reflects the imperfectness in CSI, which is equal to a sum of per-entry mean-square errors of intra- and cross-tier channel estimation during two phases. This factor goes to zero again as P_2/N_0 tends to infinity—leading to perfect CSI.

VI. NUMERICAL RESULTS

In this section, we provide some numerical results to show the effectiveness of the opportunistic IA in terms of the SINR distribution, spatial average capacity, network throughput, and energy efficiency. As illustrated in Fig. 2, we consider that the MBS is placed at the center of $\mathcal{C}$ with the area $|\mathcal{C}| = \pi r_1^2$. In addition, the MUEs are uniformly placed on the edge of a smaller circle of radius D_1 centered at the MBS. Unless specifically stated, we use the system parameters in Table II for numerical examples.

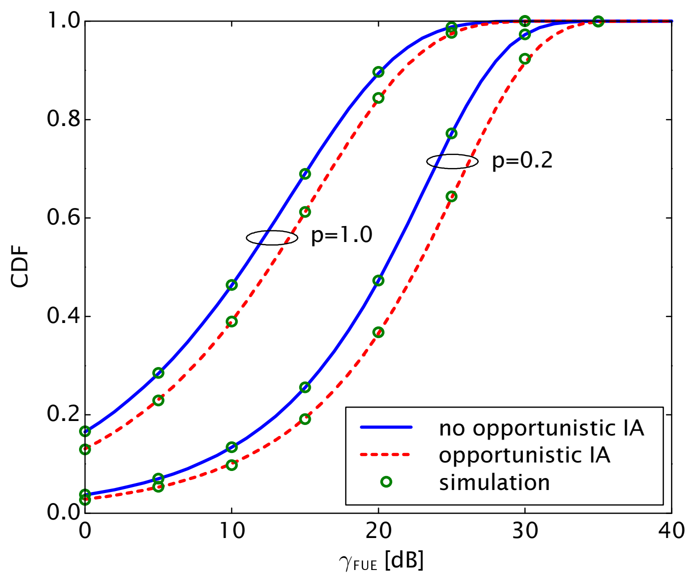

Fig. 3. CDF of the SINR $\gamma_{\rm FUE}$ at the FUE with and without opportunistic IA for $\lambda = 1.59 \times 10^{-4}$ FAPs/m^2 when $p = 0.2$ and 1.0.

Fig. 3 shows the CDF of the SINR $\gamma_{\rm FUE}$ at the FUE with and without opportunistic IA for $\lambda = 1.59 \times 10^{-4}$ FAPs/m^2 when $p = 0.2$ and 1.0. In this example, the average numbers of FAPs over the 1-Km-radius macrocell $\mathcal{C}$ are equal to 100 for $p = 0.2$ and 500 for $p = 1.0$, respectively. The case without opportunistic IA corresponds to the lower bound

$$\mathbb{P}\left\{\log_2(1+\gamma_{\rm FUE}) > \mathcal{R}\right\} \geq \int_0^\infty \exp\left[-\frac{\epsilon_{\mathcal{R}} r_2^{\alpha_2}}{r^{\alpha_3}}\left(\frac{1}{1+\eta_2/N_0}+\ell\sigma^2\right)\right] g\left(r, \epsilon_{\mathcal{R}} r_2^{\alpha_2}\right) f(r)\,dr + \left[1-\frac{2\pi\zeta}{(\zeta+2\pi)^2}\right] g\left(0, \epsilon_{\mathcal{R}} r_2^{\alpha_2}\right) \quad (61)$$

$$\langle C\rangle_{\rm FUE} \geq \int_0^\infty\int_0^\infty \exp\left[-\frac{\epsilon_t r_2^{\alpha_2}}{r^{\alpha_3}}\left(\frac{1}{1+\eta_2/N_0}+\ell\sigma^2\right)\right] g\left(r, \epsilon_t r_2^{\alpha_2}\right) f(r)\,dr dt + \left[1-\frac{2\pi\zeta}{(\zeta+2\pi)^2}\right]\int_0^\infty g\left(0, \epsilon_t r_2^{\alpha_2}\right) dt \quad (62)$$

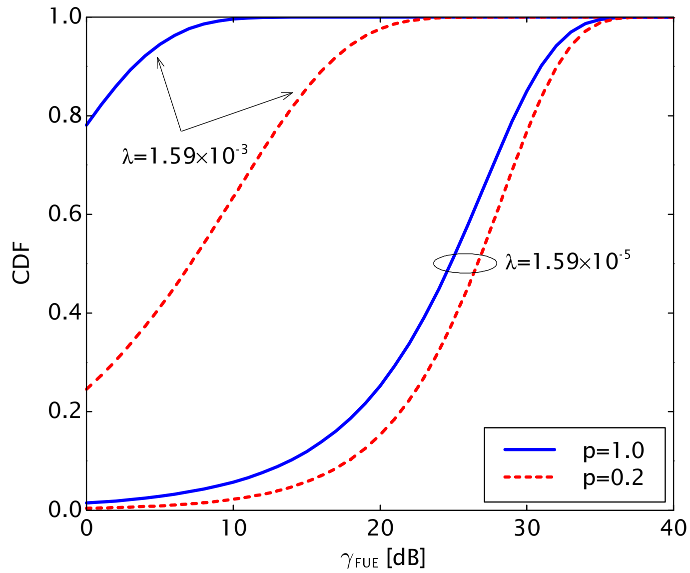

(a) FUE

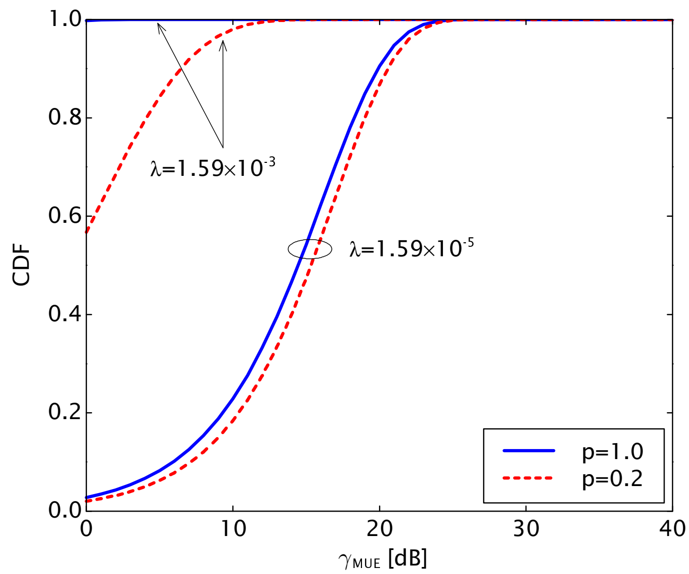

(b) MUE

Fig. 4. CDF of the SINR (a) γ_{FUE} at the FUE and (b) γ_{MUE} at the MUE with opportunistic IA for $\lambda = 1.59 \times 10^{-3}$ FAPs/m^2 (dense deployment) and $\lambda = 1.59 \times 10^{-5}$ FAPs/m^2 (sparse deployment) when $p = 0.2$ and 1.0.

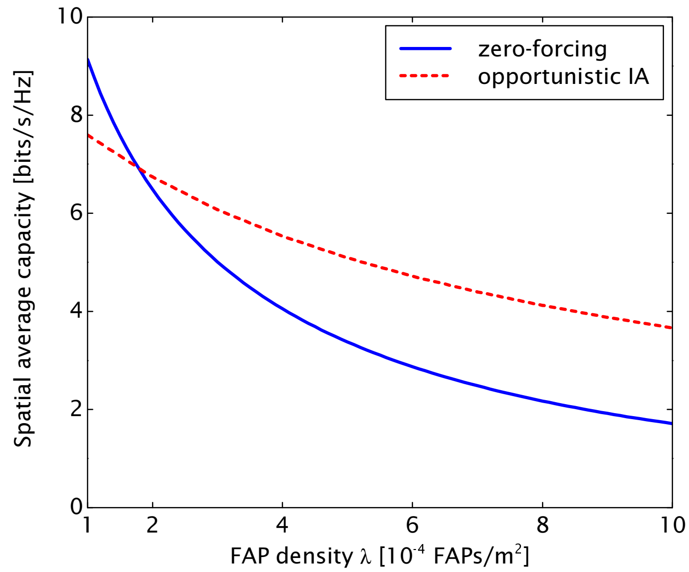

(a) FUE

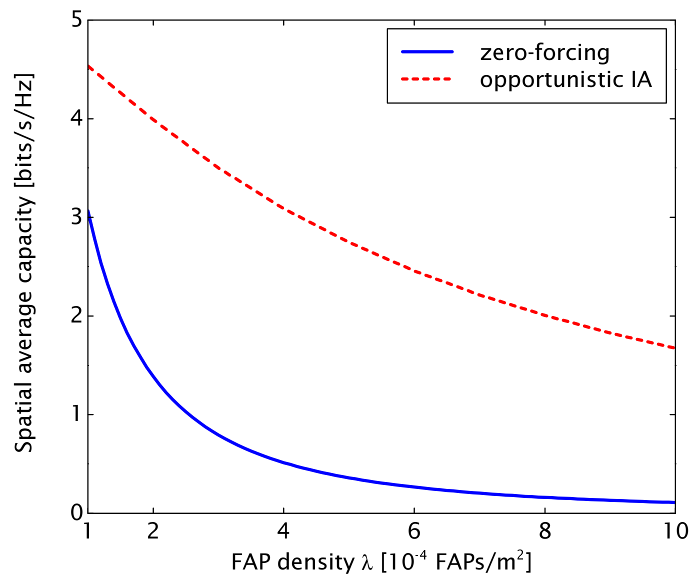

(b) MUE

Fig. 5. Spatial average capacity in bits/s/Hz at the (a) FUE and (b) MUE as a function of the FAP density λ for opportunistic IA and ZF strategies when $p = 0.2$.

(25) in Remark 3.[5] We can first see that the analyses in Theorem 2 and Remark 3 agree exactly with the simulation results, showing that the opportunistic IA increases the SINR by effectively suppressing the cross-tier interference from the macrocell and the nearest intra-tier (femtocell) interference. We observe that the random spectrum allocation ($p = 0.2$) along with opportunistic IA further improves the SINR by thinning interfering emitters, serving to capture the effect of random allocation. The effectiveness of opportunistic IA (with the random spectrum allocation) is further demonstrated in Fig. 4, where the CDFs of the SINRs γ_{FUE} at the FUE and γ_{MUE} at the MUE with opportunistic IA are depicted for $\lambda = 1.59 \times 10^{-3}$ FAPs/m^2 (dense deployment) and $\lambda = 1.59 \times 10^{-5}$ FAPs/m^2 (sparse deployment) when $p = 0.2$ and 1.0. We observe that the advantage of random spectrum allocation on reducing the intra-tier (at the FUE) or cross-tier (at the MUE) interference is more pronounced when the FAP deployment is dense.

[5]Similarly, no opportunistic IA for the MUE corresponds to the case in Remark 4.

Fig. 5 shows the spatial average capacity at the FUE and MUE as a function of the FAP density λ for opportunistic IA and ZF (see, e.g., [23]) strategies when $p = 0.2$. In [23], the ZF beamforming vector at a FUE is designed to cancel the inter-tier interference from other FUEs served by the same FAP, while in our case, TDMA transmission is used to avoid this inter-tier interference and a receive beamforming vector at the FUE is designed to cancel the intra-tier interference from the

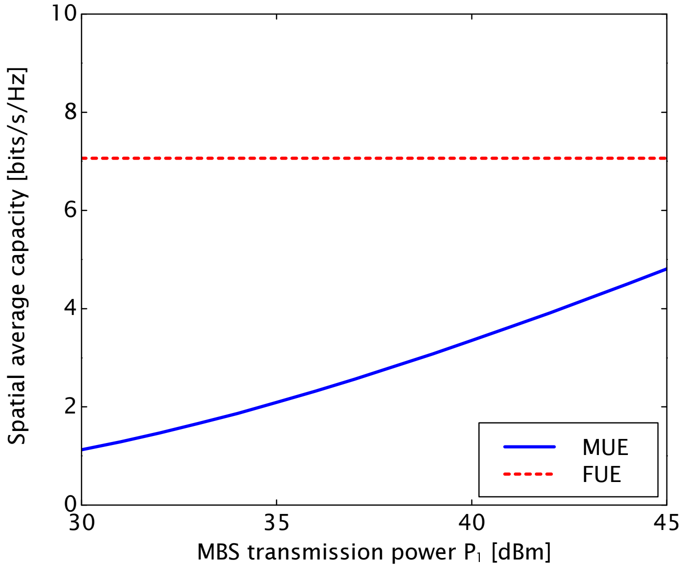

Fig. 6. Spatial average capacity in bits/s/Hz at the FUE and MUE for opportunistic IA as a function of the MBS transmission power P_1 when $\lambda = 1.59 \times 10^{-4}$ FAPs/m^2 and $p = 0.2$.

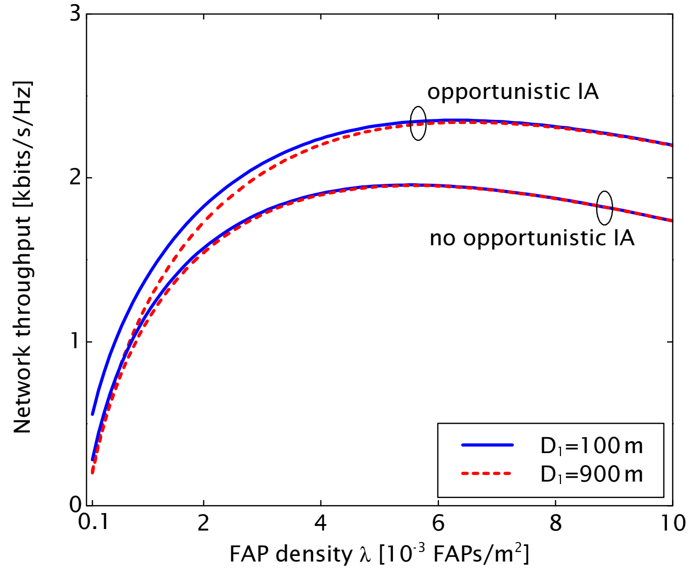

Fig. 7. Network throughput $\mathcal{T}$ in bits/s/Hz as a function of the FAP density λ with and without opportunistic IA for $p = 0.2$ when $D_1 = 100$ and 900 meters.

nearest neighboring FAP and the cross-tier interference from the MBS. We observe that the spatial average capacity for the opportunistic IA decreases less rapidly with the FAP density λ than for the ZF strategy, showing that the opportunistic IA is more beneficial to suppressing interference than the ZF as the network deployment becomes more dense. To illustrate the effect of the MBS transmission power on the achievable rate, the spatial average capacity at the FUE and MUE as a function of the MBS transmission power P_1 is plotted in Fig. 6 for opportunistic IA when $\lambda = 1.59 \times 10^{-4}$ FAPs/m^2 and $p = 0.2$, leading to 100 FAPs on average over the macrocell $\mathcal{C}$. As expected, the FUE rate remains constant due the IA capable of canceling all the cross-tier interference from the MBS, while the MUE rate increases with the MBS power P_1.

Fig. 7 shows the network throughput $\mathcal{T}$ as a function of the FAP density λ with and without opportunistic IA for $p = 0.2$ when $D_1 = 100$ and 900 meters. In this example, the optimal values of the FAP density λ that maximizes the network throughput with the opportunistic IA are equal to $\lambda^\star = 6.3 \times 10^{-3}$ FAPs/m^2 for $D_1 = 100$ and $\lambda^\star = 6.5 \times 10^{-3}$ FAPs/m^2 for $D_1 = 900$ from Theorem 4. Using the same arguments in Theorem 4 along with Remarks 3 and 4, we can also obtain the optimal value $\lambda^\star = 5.5 \times 10^{-3}$ FAPs/m^2 when $D_1 = 100$ and $\lambda^\star = 5.6 \times 10^{-3}$ FAPs/m^2 when $D_1 = 900$ for the case without opportunistic IA. We observe that as λ increases, the network throughput is dominated by the aggregate femtocell throughput and hence, the effect of the MBS-to-MUE distance D_1 is not significant. The opportunistic IA allows the network to tolerate a large number of FAPs by effectively reducing interference. The network throughput is further depicted in Fig. 8 as a function of the FAP transmission power P_2 when $\lambda = 1.59 \times 10^{-4}$ FAPs/m^2 and $p = 0.2$. We can see that $\mathcal{T}$ increases with P_2 in both cases.

Fig. 9 shows the energy efficiency $\mathcal{E}$ as a function of λ with and without opportunistic IA for $p = 0.2$ when $D_1 = 100$ and 900 meters. In this example, we set $Q_1 = 48.4$ dBm, $Q_2 = 45.3$ dBm, and $\beta_1 = \beta_2 = 5.5$ as in [21]. In this example, the optimal values of the FAP density λ that maximizes the energy efficiency with the opportunistic IA are equal to $\lambda^\star = 6.0 \times 10^{-4}$ FAPs/m^2 for $D_1 = 100$ and $\lambda^\star = 1.02 \times 10^{-3}$ FAPs/m^2 for $D_1 = 900$. We observe that as the MUEs are located closer to the MBS, the network is more energy-efficient by deploying more FAPs. Lastly, to ascertain the effect of imperfect CSI on opportunistic IA, the spatial average capacity in bits/s/Hz at the FUE is depicted in Figs. 10 and 11 as a function of the FAP transmission power P_2 and the spectrum access probability p for opportunistic IA with imperfect CSI, respectively, when $\lambda = 1.59 \times 10^{-4}$ FAPs/m^2. Specifically, we use the lower

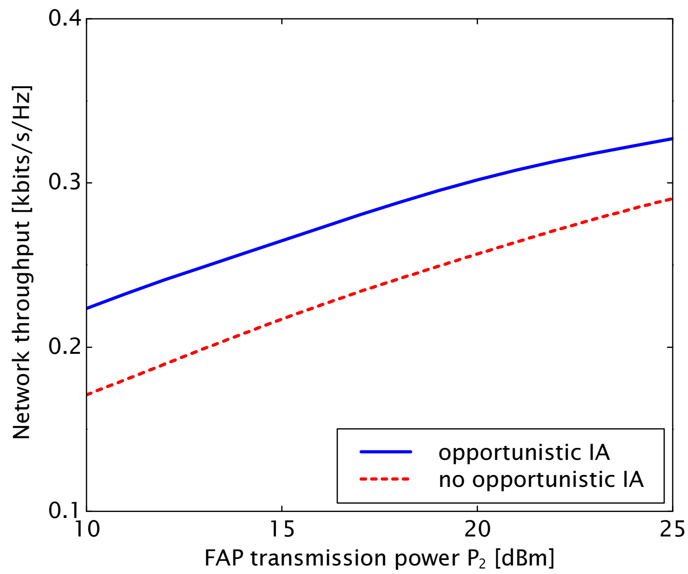

Fig. 8. Network throughput $\mathcal{T}$ in bits/s/Hz as a function of the FAP transmission power P_2 with and without opportunistic IA when $\lambda = 1.59 \times 10^{-4}$ FAPs/m^2 and $p = 0.2$.

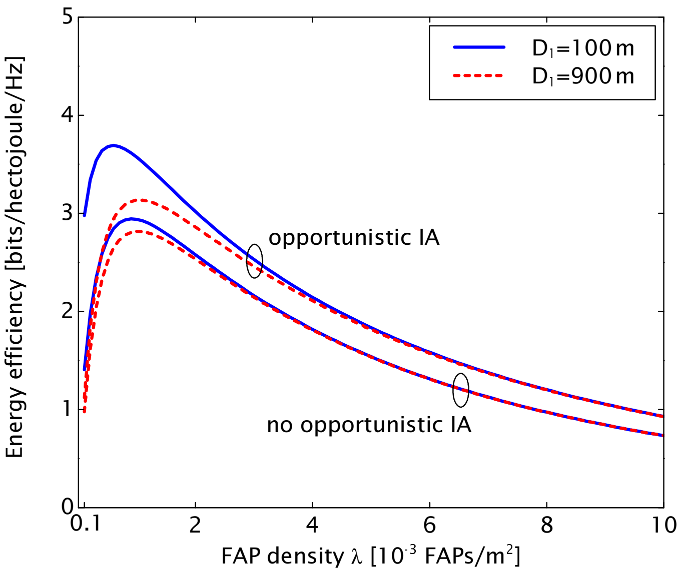

Fig. 9. Energy efficiency $\mathcal{E}$ in bits/joule/Hz as a function of the FAP density λ with and without opportunistic IA for $p = 0.2$ when $D_1 = 100$ and 900 meters. In this example, we set $Q_1 = 48.4$ dBm, $Q_2 = 45.3$ dBm, and $\beta_1 = \beta_2 = 5.5$.

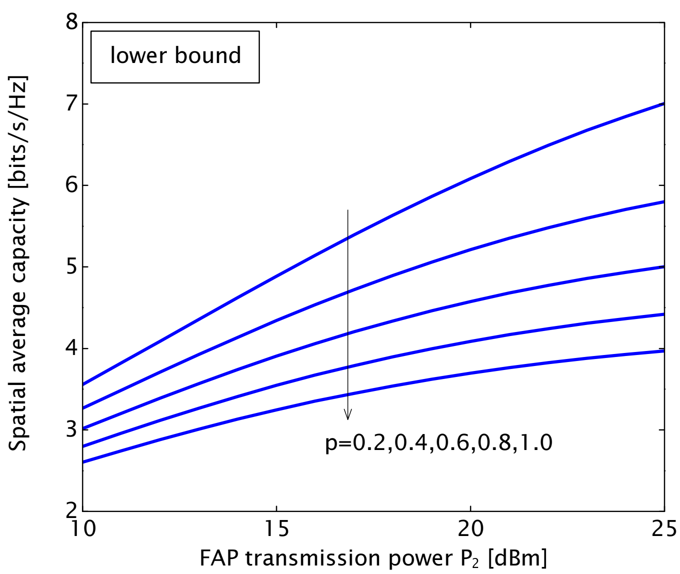

Fig. 10. Spatial average capacity in bits/s/Hz at the FUE as a function of the FAP transmission power P_2 for opportunistic IA with imperfect CSI when $p = 0.2$, 0.4, 0.6, 0.8, 1.0, and $\lambda = 1.59 \times 10^{-4}$ FAPs/m^2.

bound (62) to $\langle C \rangle_{\text{FUE}}$ in Theorem 5 for the imperfect CSI case. As expected, $\langle C \rangle_{\text{FUE}}$ increases with the FAP power P_2, while decreasing with the access probability p.

VII. Conclusion

In this paper, we investigated a two-tier downlink MIMO network, where a single MBS coexists with multiple closed-access MIMO femtocells scattered according to a homogeneous PPP. With multiple antennas at both the macrocell and femtocell users, we proposed an opportunistic IA strategy in the design of transmit and receive beamformers to suppress the intra/inter-tier and cross-tier interference. To reduce the number of macrocell and femtocell users coexisting in the same spectrum, we also employed random spectrum allocation along with the opportunistic IA. Using stochastic geometry, we evaluated the performance of our proposed scheme in terms of the SINR distribution, spatial average capacity, network throughput, and energy efficiency. With accounting for imperfect CSI at the macrocell and femtocells, we further quantified the effects of this imperfectness on the connectivity and capacity.

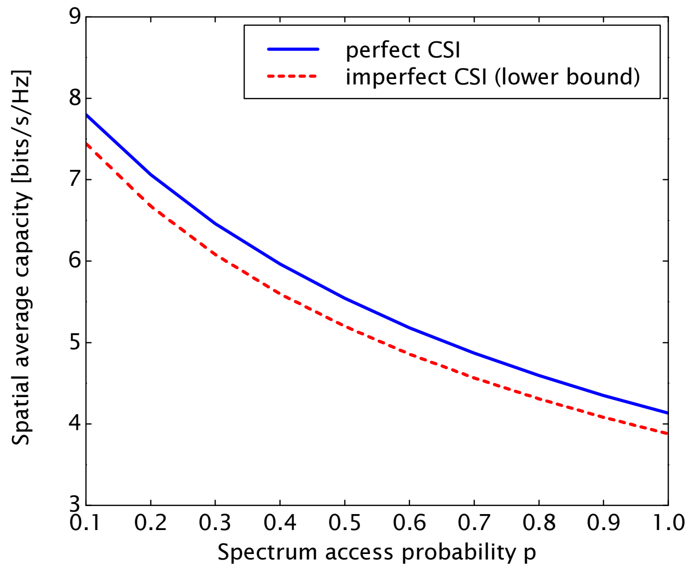

Fig. 11. Spatial average capacity in bits/s/Hz at the FUE as a function of the spectrum access probability p for opportunistic IA with perfect and imperfect CSI when $\lambda = 1.59 \times 10^{-4}$ FAPs/m^2.

Appendix

A. Feasibility of Algorithm 1

1) Feasible Condition $|\mathcal{N}_i| + 1 \le N$: In Step 1, the null space for the design (6) of $\mathbf{u}_i$ spans the dimension of $N - |\mathcal{N}_i|$. Hence, the condition (5) must be satisfied for this design.

2) Feasible Condition $N \le M_2$: It follows from the design (8) of $\mathbf{v}_j$ in Step 3 that

$$\mathbf{H}_{ij}\mathbf{v}_j = c\,\mathbf{G}_{2i}\sum_{k\in\mathcal{G}}\mathbf{f}_k \tag{65}$$

where c is a constant. The solution of $\mathbf{v}_j$ for the system equation (65) is feasible only if the number of equations N is less than and equal to the number of variables M_2.

3) Feasible Condition $(\ell - 1)\,N \le M_1$: It follows from two designs (6) and (8) that

$$\mathbf{u}_i^\dagger\mathbf{K}_{ij}\left(\mathbf{H}_{ij}^\dagger\mathbf{H}_{ij}\right)^{-1}\mathbf{H}_{ij}^\dagger\mathbf{G}_{2i}\sum_{k\in\mathcal{G}}\mathbf{f}_k = 0. \tag{66}$$

In Step 2, the design (7) of $\mathbf{f}_j$ leads to

$$\mathbf{u}_i^\dagger\mathbf{G}_{1i}\mathbf{f}_j = 0 \tag{67}$$

for $j \in \mathcal{G} \setminus \{i\}$. Combining two conditions (66) and (67), we have

$$\mathbf{K}_{ij}\left(\mathbf{H}_{ij}^\dagger\mathbf{H}_{ij}\right)^{-1}\mathbf{H}_{ij}^\dagger\mathbf{G}_{2i}\sum_{k\in\mathcal{G}}\mathbf{f}_k = \mathbf{G}_{1i}\mathbf{f}_j \tag{68}$$

which is equivalent to

$$\mathbf{K}_{ij}\left(\mathbf{H}_{ij}^{\dagger}\mathbf{H}_{ij}\right)^{-1}\mathbf{H}_{ij}^{\dagger}\mathbf{G}_{2i}\left(\mathbf{f}_i+\sum_{k\in\mathcal{G}\setminus\{i,j\}}\mathbf{f}_k\right)+\left[\mathbf{K}_{ij}\left(\mathbf{H}_{ij}^{\dagger}\mathbf{H}_{ij}\right)^{-1}\mathbf{H}_{ij}^{\dagger}\mathbf{G}_{2i}-\mathbf{G}_{1i}\right]\mathbf{f}_j=0. \quad (69)$$

Hence, there are $\ell(\ell-1)N$ equations and ℓM_1 variables, leading to the feasible condition (11).

B. Proof of Theorem 2

The PDF of the nearest distance $R_{2i^\star}$ for the homogeneous PPP Π with intensity $p\lambda$ is given by [18], [19]

$$p_{R_{2i^\star}}(r)=2\pi p\lambda r\exp\left(-\pi p\lambda r^2\right),\quad r\geq 0. \quad (70)$$

Following [24], we can obtain the conditional MGF of $I_{\mathrm{FUE}}(\Omega)$ given $R_{2i^\star}$ for $\Omega=\Pi\setminus\{0,i^\star\}$ as follows:

$$\phi_{I_{\mathrm{FUE}}(\Omega)|R_{2i^\star}}\left(s\middle|R_{2i^\star}\right)=\exp\left[-2\pi p\lambda s\left(1-\frac{R_{2i^\star}^2}{r_1^2}\right)\int_{R_{2i^\star}}^{r_1}\frac{tdt}{s+t^{\alpha_3}}\right]. \quad (71)$$

Note that the integral in the exponent of (71) can be evaluated as incomplete gamma functions. For $\Omega=\Pi\setminus\{0\}$, (71) reduces to

$$\phi_{I_{\mathrm{FUE}}(\Omega)|R_{2i^\star}}\left(s\middle|R_{2i^\star}\right)=\phi_{I_{\mathrm{FUE}}(\Omega)}(s)=\exp\left(-2\pi p\lambda s\int_0^{r_1}\frac{tdt}{s+t^{\alpha_3}}\right). \quad (72)$$

Using Theorem 1 and (70)–(72), we get (73), as shown at the bottom of the page, and

$$\begin{aligned}\mathbb{P}\{\gamma_{\mathrm{FUE}}\geq z,\mathcal{A}^c\}&=\mathbb{P}\left\{\gamma_{\mathrm{FUE}}\geq z\middle|\mathcal{A}^c\right\}(1-\mathbb{P}\{\mathcal{A}\})\\&=g\left(0,zr_2^{\alpha_2}\right)\Bigg[1-\underbrace{p\lambda\zeta\,\mathbb{E}_{R_{2i^\star}}\left\{R_{2i^\star}^2\exp\left(-p\lambda\zeta R_{2i^\star}^2\right)\right\}}_{=\frac{2\pi\zeta}{(\zeta+2\pi)^2}}\Bigg].\end{aligned} \quad (74)$$

By substituting (73) and (74) into (19), we arrive at the desired result (21).

Since $\mathbb{E}\{X\}=\int_0^\infty\mathbb{P}\{X>t\}\,dt$ for a nonnegative RV X, the spatial average capacity of the FUE can be written as

$$\langle C\rangle_{\mathrm{FUE}}=\mathbb{E}\{\log_2(1+\gamma_{\mathrm{FUE}})\}=\int_0^\infty\left[1-F_{\gamma_{\mathrm{FUE}}}(\epsilon_t)\right]dt \quad (75)$$

from which and (21) we complete the proof.

C. Proof of Theorem 4

We first show that $\mathcal{T}_{\mathrm{MUE}}$ as a function of $\lambda\in[0,\infty)$ is concave. Let

$$\psi(\lambda,r,s)=\lambda^{|\mathcal{N}_0|}e^{-\pi p\lambda r^2}g(r,s). \quad (76)$$

Then, since $\psi(\lambda,r,s)$ is positive for every $\lambda,r,s\in[0,\infty)$, it is sufficient to show that $\psi(\lambda,r,s)$ is concave in $\lambda\in[0,\infty)$. Note that

$$\frac{\partial\psi(\lambda,r,s)}{\partial\lambda}=e^{-\pi p\lambda r^2}g(r,s)\,\lambda^{|\mathcal{N}_0|-1}\times\left[|\mathcal{N}_0|-\pi p\lambda r^2+\ln g(r,s)\right] \quad (77)$$

Since $\partial\psi(\lambda,r,s)/\partial\lambda$ in (77) has a unique root at

$$\lambda_1=|\mathcal{N}_0|\left[\pi pr^2+2\pi ps\left(1-\frac{r^2}{r_1^2}\right)\int_r^{r_1}\frac{tdt}{s+t^{\alpha_3}}+\frac{sN_0}{P_2}\right]^{-1} \quad (78)$$

and

$$\left[\frac{\partial^2\psi(\lambda,r,s)}{\partial\lambda^2}\right]\Bigg|_{\lambda=\lambda_1}=-e^{-|\mathcal{N}_0|}\lambda_1^{|\mathcal{N}_0|-2}|\mathcal{N}_0|<0 \quad (79)$$

it follows that $\psi(\lambda,r,s)$ is concave in $\lambda\in[0,\infty)$. Using the same arguments and the fact that $\lambda g(r,s)$ as a function of $\lambda\in[0,\infty)$ is concave for every $r,s\in[0,\infty)$, we can show that $pL\mathcal{T}_{\mathrm{FUE}}$ is a concave function in $\lambda\in[0,\infty)$. Hence, we complete the proof.

D. Proof of Theorem 5

Taking into account imperfect CSI in the opportunistic IA in Algorithm 1, the designs of transmit beamforming vectors at the MBS and FAPs are given by

$$\mathbf{f}_i\in\mathsf{Null}\left(\bigcup_{j\in\mathcal{G},\,j\neq i}\mathbf{u}_j^{\dagger}\widehat{\mathbf{G}}_{1j}\right) \quad (80)$$

$$\mathsf{Span}\left(\widehat{\mathbf{H}}_{ij}\mathbf{v}_j\right)=\mathsf{Span}\left(\widehat{\mathbf{G}}_{2i}\sum_{k\in\mathcal{G}}\mathbf{f}_k\right). \quad (81)$$

These imperfect-CSI counterparts only affect the intra-tier interference from the nearest interfering FAP in (12) as follows:

$$\begin{aligned}\mathbf{w}_0^{\dagger}\mathbf{H}_{0i^\star}\mathbf{v}_{i^\star}&=\mathbf{w}_0^{\dagger}\widehat{\mathbf{H}}_{0i^\star}\mathbf{v}_{i^\star}+\mathbf{w}_0^{\dagger}\widetilde{\mathbf{H}}_{0i^\star}\mathbf{v}_{i^\star}\\&\overset{(a)}{=}\mathbf{w}_0^{\dagger}\widehat{\mathbf{G}}_{20}\sum_{k\in\mathcal{G}}\mathbf{f}_k+Z\\&\overset{(b)}{=}\mathbf{w}_0^{\dagger}\left(\mathbf{G}_{20}-\widetilde{\mathbf{G}}_{20}\right)\sum_{k\in\mathcal{G}}\mathbf{f}_k+Z\\&\overset{(c)}{=}-\sum_{k\in\mathcal{G}}\mathbf{w}_0^{\dagger}\widetilde{\mathbf{G}}_{20}\mathbf{f}_k+Z\end{aligned} \quad (82)$$

$$\begin{aligned}\mathbb{P}\{\gamma_{\mathrm{FUE}}\geq z,\mathcal{A}\}&=\mathbb{E}_{R_{2i^\star}}\left\{\mathbb{P}\left\{\gamma_{\mathrm{FUE}}\geq z\middle|\mathcal{A},R_{2i^\star}\right\}\mathbb{P}\left\{\mathcal{A}\middle|R_{2i^\star}\right\}\right\}\\&=p\lambda\zeta\exp\left(-zr_2^{\alpha_2}N_0/P_2\right)\cdot\mathbb{E}_{R_{2i^\star}}\left\{\phi_{I_{\mathrm{FUE}}(\Omega)|R_{2i^\star}}\left(zr_2^{\alpha_2}\middle|R_{2i^\star}\right)R_{2i^\star}^2\exp\left(-p\lambda\zeta R_{2i^\star}^2\right)\right\}\\&=\int_0^\infty f(r)\,g\left(r,zr_2^{\alpha_2}\right)dr\end{aligned} \quad (73)$$

where (a) follows from (81) and defining $Z \triangleq \mathbf{w}_0^{\dagger}\widetilde{\mathbf{H}}_{0i^\star}\mathbf{v}_{i^\star}$; (b) follows by denoting the estimation error as $\widetilde{\mathbf{G}}_{20} = \mathbf{G}_{20} - \widehat{\mathbf{G}}_{20}$; and (c) follows from (10). Since the entries of $\widetilde{\mathbf{H}}_{0i^\star}$ are independent Gaussian $\mathcal{CN}\big(0, \frac{1}{1+\eta_2/N_0}\big)$ and the mean-square error for each entry of $\widehat{\mathbf{G}}_{2i}$ in (60) is equal to σ^2 (see, e.g., [22]), letting $W_k = -\mathbf{w}_0^{\dagger}\widetilde{\mathbf{G}}_{20}\mathbf{f}_k$, we have

$$\mathbb{E}\left\{|Z|^2\right\} = \frac{1}{1+\eta_2/N_0} \tag{83}$$

$$\mathbb{E}\left\{|W_k|^2\right\} = \sigma^2. \tag{84}$$

Using (82) and taking the same steps to lead the SINR distribution in Theorem 2, we obtain the SINR distribution at the typical FUE for the imperfect CSI case as follows:

$$\begin{aligned} &F_{\gamma_{\text{FUE}}}(z) \\ &= 1 - \int_0^\infty f(r)\, g\left(r, z r_2^{\alpha_2}\right) \phi_{|Z|^2 + \sum_{k\in\mathcal{G}}|W_k|^2}\left(\frac{z r_2^{\alpha_2}}{r^{\alpha_1}}\right) dr \\ &\quad - \left[1 - \frac{2\pi\zeta}{(\zeta+2\pi)^2}\right] g\left(0, z r_2^{\alpha_2}\right), \qquad z \geq 0. \end{aligned} \tag{85}$$

Since the distribution of $|W_k|^2$ is unknown, we apply Jensen's inequality to the MGF in (85) as follows:

$$\begin{aligned} \phi_{|Z|^2+\sum_{k\in\mathcal{G}}|W_k|^2}\left(\frac{z r_2^{\alpha_2}}{r^{\alpha_3}}\right) &= \mathbb{E}\left\{e^{-\frac{z r_2^{\alpha_2}}{r^{\alpha_3}}\left(|Z|^2+\sum_{k\in\mathcal{G}}|W_k|^2\right)}\right\} \\ &\geq e^{-\frac{z r_2^{\alpha_2}}{r^{\alpha_3}}\left(\mathbb{E}\{|Z|^2\}+\sum_{k\in\mathcal{G}}\mathbb{E}\{|W_k|^2\}\right)}. \end{aligned} \tag{86}$$

From (83)–(86) and the fact that $|\mathcal{G}| = \ell$, we complete the proof.

References

[1] Y. Chen, S. Zhang, S. Xu, and G. Y. Li, "Fundamental trade-offs on green wireless networks," *IEEE Commun. Mag.*, vol. 49, no. 6, pp. 30–37, Jun. 2011.

[2] D. López-Pérez, I. Gúvenc, G. de la Roche, M. Kountouris, T. Q. S. Quek, and J. Zhang, "Enhanced intercell interference coordination challenges in heterogeneous networks," *IEEE Wireless Commun. Mag.*, vol. 18, no. 3, pp. 22–30, Jun. 2011.

[3] V. Chandrasekhar, J. G. Andrews, and A. Gatherer, "Femtocell networks: A survey," *IEEE Commun. Mag.*, vol. 46, no. 9, pp. 59–67, Sep. 2008.

[4] D. Calin, H. Claussen, and H. Uzunalioglu, "On femto deployment architectures and macrocell offloading benefits in joint macro-femto deployments," *IEEE Commun. Mag.*, vol. 48, no. 1, pp. 26–32, Jan. 2010.

[5] A. Rabbachin, T. Q. S. Quek, H. Shin, and M. Z. Win, "Cognitive network interference," *IEEE J. Sel. Areas Commun.*, vol. 29, no. 2, pp. 480–493, Feb. 2011.

[6] S.-M. Cheng, S.-Y. Lien, F.-S. Chu, and K.-C. Chen, "On exploiting cognitive radio to mitigate interference in macro/femto heterogeneous networks," *IEEE Wireless Commun. Mag.*, vol. 18, no. 3, pp. 40–47, Jun. 2011.

[7] Y. Jeong, T. Q. S. Quek, and H. Shin, "Beamforming optimization for multiuser two-tier networks," *J. Commun. and Networks*, vol. 13, no. 4, pp. 327–338, Aug. 2011.

[8] Y. Jeong, H. Shin, and M. Z. Win, "Superanalysis of optimum combining with application to femtocell networks," *IEEE J. Sel. Areas Commun.*, vol. 30, no. 3, pp. 509–524, Apr. 2012.

[9] P. Xia, V. Chandrasekhar, and J. G. Andrews, "Open vs. closed access femtocells in the uplink," *IEEE Trans. Wireless Commun.*, vol. 9, no. 12, pp. 3798–3809, Dec. 2010.

[10] W. C. Cheung, T. Q. S. Quek, and M. Kountouris, "Throughput Optimization, Spectrum Allocation, and Access Control in Two-Tier Femtocell Networks," *IEEE J. Sel. Areas Commun.*, vol. 30, no. 3, pp. 561–574, Apr. 2012.

[11] V. R. Cadambe and S. A. Jafar, "Interference alignment and degrees of freedom of the K-user interference channel," *IEEE Trans. Inf. Theory*, vol. 54, no. 8, pp. 3425–3441, Aug. 2008.

[12] C. Huang and S. A. Jafar, "Degrees of freedom of the MIMO interference channel with cooperation and cognition," *IEEE Trans. Inf. Theory*, vol. 55, no. 9, pp. 4211–4220, Sep. 2009.

[13] C.-B. Chae, S.-H. Kim, and R. W. Heath Jr., "Network coordinated beamforming for cell-boundary users: Linear and nonlinear approaches," *IEEE J. Select. Topics Signal Process.*, vol. 3, no. 6, pp. 1094–1105, Dec. 2009.

[14] S. M. Perlaza, N. Fawaz, S. Lasaulce, and M. Debbah, "From spectrum pooling to space pooling: Opportunistic interference alignment in MIMO cognitive networks," *IEEE Trans. Signal Process.*, vol. 58, no. 7, pp. 3728–3741, Jul. 2010.

[15] W. Shin, N. Lee, W. Noh, H.-H. Choi, B. Clerckx, C. Shin, and K. Jang, "Hierarchical interference alignment for heterogeneous networks with multiple antennas," in *Proc. IEEE Int. Conf. Communications (ICC'11)*, Kyoto, Japan, Jun. 2011, pp. 1–6.

[16] C. Suh, M. Ho, and D. N. C. Tse, "Downlink interference alignment," *IEEE Trans. Commun.*, vol. 59, no. 9, pp. 2616–2626, Sep. 2011.

[17] A. Adhikary, V. Ntranos, and G. Caire, "Cognitive femtocells: Breaking the spatial reuse barrier of cellular systems," in *Proc. IEEE Int. Theory and Applications Workshop (ITA'11)*, San Diego, CA, Feb. 2011, pp. 1–10.

[18] M. Haenggi, "On distances in uniformly random networks," *IEEE Trans. Inf. Theory*, vol. 51, no. 10, pp. 3584–3586, Oct. 2005.

[19] Y. Jeong, H. Shin, and M. Z. Win, "Intervehicle communication: Cox–Fox modeling," *IEEE J. Sel. Areas Commun.*, to be published.

[20] A. Goldsmith, *Wireless Communications*. Cambridge, UK: Cambridge University Press, 2005.

[21] W. Wang and G. Shen, "Energy efficiency of heterogeneous cellular network," in *Proc. IEEE Veh. Technol. Conf. (VTC'10 Fall)*, Ottawa, Canada, Sep. 2010, pp. 1–5.

[22] O. E. Ayach and R. W. Heath Jr., "Interference alignment with analog CSI feedback," in *Proc. IEEE Military Commun. Conf. (MILCOM'10)*, San Jose, CA, Oct. 2010, pp. 1644–1648.

[23] V. C. Chandrasekhar, M. Kountouris, and J. G. Andrews, "Coverage in multi-antenna two-tier networks," *IEEE Trans. Wireless Commun.*, vol. 8, no. 10, pp. 5314–5327, Oct. 2009.

[24] S. P. Weber, J. G. Andrews, X. Yang, and G. de Veciana, "Transmission capacity of wireless ad hoc networks with successive interference cancellation," *IEEE Trans. Inf. Theory*, vol. 53, no. 8, pp. 2799–2814, Aug. 2007.

Tri Minh Nguyen (S'10) received the B.C. degree in Electrical Engineering from Ho Chi Minh City University of Technology, Vietnam, in 2009, and the M.E. degree in Electrical Engineering from Kyung Hee University, Yongin, Korea, in 2012. His current research interests include interference in heterogeneous networks and wireless cooperative localization.

Youngmin Jeong (S'09) received the B.E. and M.E. degrees in Electronics and Radio Engineering from Kyung Hee University, Yongin, Korea, in 2009 and 2011, respectively. He is currently working toward the Ph.D. degree in Electronics and Radio Engineering at Kyung Hee University. His current research interests include wireless communications, cooperative communications, and heterogeneous networks.

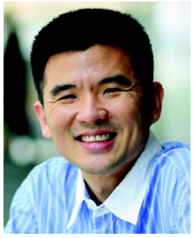

Tony Q.S. Quek (S'98-M'08-SM'12) received the B.E. and M.E. degrees in Electrical and Electronics Engineering from Tokyo Institute of Technology, Tokyo, Japan, in 1998 and 2000, respectively. At Massachusetts Institute of Technology (MIT), Cambridge, MA, he earned the Ph.D. in Electrical Engineering and Computer Science in Feb. 2008.

Currently, he is an Assistant Professor with the Information Systems Technology and Design Pillar at Singapore University of Technology and Design (SUTD). He is also a Scientist with the Institute for Infocomm Research. His main research interests are the application of mathematical, optimization, and statistical theories to communication, networking, signal processing, information theoretic, and resource allocation problems. Specific current research topics include cooperative networks, interference networks, heterogeneous networks, green communications, smart grid, wireless security, localization, compressed sensing, and cognitive radio.

Dr. Quek has been actively involved in organizing and chairing sessions, and has served as a member of the Technical Program Committee (TPC) in a number of international conferences. He served as the Cognitive Radio & Cooperative Communications Track Chair for the IEEE VTC in spring 2011, the Wireless Communications Symposium Chair for the IEEE Globecom in 2011, and the Communication Theory Symposium Chair for the IEEE WCSP in 2013. He is currently an Editor for the IEEE TRANSACTIONS ON COMMUNICATIONS, and the IEEE WIRELESS COMMUNICATIONS LETTERS. He was Guest Editor for the JOURNAL OF COMMUNICATIONS AND NETWORKS (Special Issue on Heterogeneous Networks) in 2011, and the IEEE COMMUNICATIONS MAGAZINE (Special Issue on Heterogeneous and Small Cell Networks) in 2013.

Dr. Quek received the Singapore Government Scholarship in 1993, Tokyu Foundation Fellowship in 1998, and the A*STAR National Science Scholarship in 2002. He was honored with the 2008 Philip Yeo Prize for Outstanding Achievement in Research, the IEEE Globecom 2010 Best Paper Award, the 2011 JSPS Invited Fellow for Research in Japan, the CAS Fellowship for Young International Scientists in 2011, and the 2012 IEEE William R. Bennett Prize.

Wee Peng Tay (S'06-M'08) received the B.S. degree in electrical engineering and mathematics, and the M.S. degree in electrical engineering from Stanford University in 2002. He received the Ph.D. degree in electrical engineering and computer science from the Massachusetts Institute of Technology in 2008. He is currently an Assistant Professor in the School of Electrical and Electronics Engineering at Nanyang Technological University in Singapore.

He received the Singapore Technologies Scholarship in 1998, the Stanford University President's Award in 1999, and the Frederick Emmons Terman Engineering Scholastic Award in 2002. He is the co-author of the best student paper award at the 46th Asilomar Conference on Signals, Systems, and Computers. His research interests include distributed decision making, data fusion, distributed algorithms, communications in ad hoc networks, machine learning and applied probability.

Hyundong Shin (S'01-M'04-SM'11) received the B.S. degree in Electronics Engineering from Kyung Hee University, Korea, in 1999, and the M.S. and Ph.D. degrees in Electrical Engineering from Seoul National University, Seoul, Korea, in 2001 and 2004, respectively.

From September 2004 to February 2006, Dr. Shin was a Postdoctoral Associate at the Laboratory for Information and Decision Systems (LIDS), Massachusetts Institute of Technology (MIT), Cambridge, MA, USA. In 2006, he joined Kyung Hee University, Korea, where he is now an Associate Professor at the Department of Electronics and Radio Engineering. His research interests include wireless communications and information theory with current emphasis on MIMO systems, cooperative and cognitive communications, network interference, vehicular communication networks, and intrinsically secure networks.

Professor Shin has served as a member of the Technical Program Committee (TPC) in a number of international conferences. He served as the Technical Program Co-chair for the PHY Track of the IEEE Wireless Communications and Networking Conference (WCNC) in 2009 and the Communication Theory Symposium of the IEEE Global Communications Conference (Globecom) in 2012. Dr. Shin is currently an Editor for the IEEE TRANSACTIONS ON WIRELESS COMMUNICATIONS and the KSII Transactions on Internet and Information Systems. He was a Guest Editor for the EURASIP Journal on Advances in Signal Processing (Special Issue on Wireless Cooperative Networks) in 2008.

Professor Shin was honored with the Knowledge Creation Award in the field of Computer Science from Korean Ministry of Education, Science and Technology in 2010. He received the IEEE Communications Society William R. Bennett Prize Paper Award (2012), Guglielmo Marconi Prize Paper Award (2008), the IEEE Vehicular Technology Conference (VTC) Best Paper Award in Spring 2008, and the IEEE VTS APWCS Best Paper Award in 2010.